

Hydrogen Adsorption by Alkali Metal Graphite Intercalation Compounds

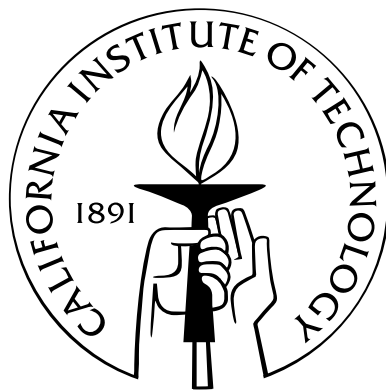
Thesis by

Justin Purewal

In Partial Fulfillment of the Requirements

for the Degree of

Doctor of Philosophy



California Institute of Technology

Pasadena, California

2010

(Defended February 9, 2010)

© 2010

Justin Purewal

All Rights Reserved

Acknowledgements

There are many people that I would like to acknowledge for their help during my Ph.D. studies. First, I thank my thesis advisor, Prof. Brent Fultz, for his exceptionally thoughtful guidance and advice. It has been a privilege, and also a pleasure, to be able to discuss research with such a distinguished scientist each week. I am also deeply indebted to my co-advisor, Dr. Channing Ahn. In addition to providing exciting research projects to work on, he has also provided a great deal of practical research knowledge.

There are many people at Caltech who helped to teach me new research techniques. I particularly thank Carol Garland for her time and patience in teaching me how to use the TEM. Other people to whom I owe gratitude include: Sonjong Hwang, for collecting the NMR measurements; Liz Miura, for collecting the Raman measurements; Houria Kabbour, who taught me how to use the Sieverts instrument and was always happy to answer my many questions; Mike Vondrus, for machining a number of neutron scattering sample cans; Itzhak Halevy, for providing insight into high-pressure spectroscopy measurements; Brandon Keith, for extensive help with the molecular dynamics simulations, particularly in setting up the potentials, and for the help in answering my many UNIX-related questions. Max, Nick and Hillary, thanks for your help and company during the long trips to national labs. I also wish to express gratitude to the other current Fultz group members: David, Hongjin, Lisa, Jorge, Kun-Woo, Chen, and Mike. Lunch-times and conversations were always fun.

There are many outside collaborators who also need to be thanked, particularly Craig Brown and Madhu Tyagi at the NIST Center for Neutron Research. They played a huge role in helping me collect and interpret the neutron scattering data reported in this thesis. I owe a great deal of gratitude to Ron Cappelletti (NIST), who was happy to discuss the honeycomb jump diffusion model with me, and also made available some of his old computer codes for performing the fits. Also, I would like to thank Jason Simmons for helping with the isotherm measurements at NCNR. Lastly, I thank my family for their constant support over the years.

Financial support for this thesis was provided by the U. S. Department of Energy.

Abstract

Adsorption occurs whenever a solid surface is exposed to a gas or liquid, and is characterized by an increase in fluid density near the interface. Adsorbents have attracted attention in the ongoing effort to engineer materials that store hydrogen at high densities within moderate temperature and pressure regimes. Carbon adsorbents are a logical choice as a storage material due to their low costs and large surface areas. Unfortunately, carbon adsorbents suffer from a low binding enthalpy for H_2 (about 5 kJ mol^{-1}), well below the 15 to 18 kJ mol^{-1} that is considered optimal for hydrogen storage systems. Binding interactions can be increased by the following methods: (1) adjusting the graphite interplanar separation with a pillared structure, and (2) introducing dopant species that interact with H_2 molecules by strong electrostatic forces. Graphite intercalation compounds are a class of materials that contain both pillared structures and chemical dopants, making them an excellent model system for studying the fundamentals of hydrogen adsorption in nanostructured carbons.

Pressure-composition-temperature diagrams of the $\text{MC}_{24}(\text{H}_2)_x$ graphite intercalation compounds were measured for $\text{M} = (\text{K}, \text{Rb}, \text{Cs})$. Adsorption enthalpies were measured as a function of H_2 concentration. Notably, CsC_{24} had an average adsorption enthalpy of 14.9 kJ mol^{-1} , nearly three times larger than that of pristine graphite. The adsorption enthalpies were found to be positively correlated with the interlayer spacing. Adsorption capacities were negatively correlated with the size of the alkali metal. The rate of adsorption

is reduced at large H_2 compositions, due to the effects of site-blocking and correlation on the H_2 diffusion.

The strong binding interaction and pronounced molecular-sieving behavior of KC_{24} is likely to obstruct the translational diffusion of adsorbed H_2 molecules. In this work, the diffusivity of H_2 adsorbed in KC_{24} was studied by quasielastic neutron scattering measurements and molecular dynamics simulations. As predicted, the rate of diffusion in KC_{24} is over an order of magnitude slower than in other carbon sorbents (e.g. carbon nanotubes, nanohorns and carbon blacks). It is similar in magnitude to the rate of H_2 diffusion in zeolites with molecular-sized cavities. This suggests that H_2 diffusion in adsorbents is influenced very strongly by the pore geometry, and less strongly by the chemical nature of the pore surface. Furthermore, the H_2 diffusion mechanism in KC_{24} is complex, with the presence of at least two distinct jump frequencies.

Bound states of adsorbed H_2 in KC_{24} were investigated by inelastic neutron scattering measurements and first-principles DFT calculations. Spectral peaks in the neutron energy loss range of 5 meV to 45 meV were observed for the first time. These peaks were interpreted as single- and multi-excitation transitions of the H_2 phonon and rotational modes. The rotational barrier for H_2 molecules is many times larger in KC_{24} than in other carbon adsorbents, apparently due to the confinement of the molecules between closely-spaced graphitic layers. Evidence was found for the existence of at least three H_2 sorption sites in KC_{24} , each with a distinctive rotational barrier.

Contents

Acknowledgements	iii
Abstract	v
1 Hydrogen Storage Materials	1
1.1 Introduction	1
1.2 Physical storage of hydrogen	2
1.3 Technical targets for hydrogen storage materials	3
1.4 Storage based on physisorption	4
1.5 The mechanism of physisorption	7
1.5.1 Overview	7
1.5.2 Dispersion interactions	8
1.5.3 Electrostatic interactions	10
1.5.4 Orbital interactions	11
1.6 Carbon adsorbents	12
1.6.1 Overview	12
1.6.2 Graphite	12
1.6.3 Fullerenes	15
1.6.4 Activated Carbons	16

1.6.5	Zeolites	17
1.6.6	Metal-organic frameworks	17
1.6.7	Hydrogen adsorption by porous carbons	18
1.6.8	Chemically modified carbon adsorbents	20
1.7	Conclusion	21
2	Potassium Intercalated Graphite	22
2.1	Introduction	22
2.2	History	22
2.3	Structure of potassium-intercalated graphite	25
2.3.1	Stacking sequence	25
2.3.2	In-plane potassium structure	26
2.4	Properties of potassium-intercalated graphite	29
2.5	Synthesis of KC_{24} samples	30
2.6	Characterization of KC_{24} samples	32
2.6.1	Powder X-ray diffraction	32
2.6.2	Raman spectroscopy	36
2.6.3	Neutron diffraction	36
3	Experimental Methods	40
3.1	Gas Adsorption Measurements	40
3.1.1	Introduction	40
3.1.2	Theoretical framework	40
3.1.2.1	Surface excess adsorption	40
3.1.2.2	Thermodynamics	43

3.1.2.3	Isosteric heat of adsorption	44
3.1.2.4	Henry's law	47
3.1.3	Sieverts apparatus	49
3.1.3.1	Description	49
3.1.3.2	Volumetric method	51
3.1.3.3	Errors in volumetric adsorption measurements	53
3.2	Neutron scattering	55
3.2.1	Introduction	55
3.2.2	Theory	56
3.2.3	Indirect geometry spectrometers	60
3.2.4	Direct geometry spectrometers	61
4	Hydrogen adsorption by graphite intercalation compounds	62
4.1	Introduction	62
4.2	Hydrogen adsorption isotherms of KC_{24}	63
4.3	Hydrogen adsorption isotherms of RbC_{24} and CsC_{24}	66
4.4	Hydrogen adsorption kinetics	69
4.5	Discussion	70
4.6	Conclusion	71
5	Hydrogen diffusion in potassium-intercalated graphite	73
5.1	Introduction	73
5.2	Quasielastic neutron scattering	74
5.2.1	Description	74
5.2.2	Continuous diffusion	74

5.2.3	Jump diffusion	75
5.2.4	Concentration effects	77
5.3	Experimental methods	78
5.4	Quasielastic scattering results	79
5.5	Honeycomb lattice diffusion model	80
5.6	Estimates of diffusion coefficients	90
5.6.1	Low- Q limit	90
5.6.2	High- Q limit	92
5.6.3	Distribution of jump frequencies	94
5.7	Measurements at longer timescales	97
5.7.1	Overview	97
5.7.2	Methods	97
5.7.3	Quasielastic scattering	98
5.7.4	Elastic intensity	98
5.8	Molecular dynamics simulations	101
5.8.1	Computational details	101
5.8.2	Results	103
5.8.3	Concentration effects	106
5.9	Discussion	109
5.9.1	Comparison with carbons, zeolites, and MOFs	109
5.9.2	Diffusion on two time-scales	110
5.9.3	Phase transformations	111
5.10	Conclusions	113

6	Hydrogen binding sites in potassium intercalated graphite	114
6.1	Introduction	114
6.2	Background	115
6.2.1	Rotational energy levels of the free hydrogen molecule	115
6.2.2	Ortho- and para-hydrogen	115
6.2.3	One-dimensional hindered diatomic rotor	116
6.2.4	Scattering law for rotational transitions of molecular hydrogen	118
6.3	Experimental methods	120
6.4	Results	124
6.4.1	Low-energy IINS spectra	124
6.4.2	Diffraction pattern from low-energy IINS spectra	125
6.4.3	Intermediate and high-energy IINS spectra	126
6.4.4	IINS spectra of HD and D ₂ adsorbed in KC ₂₄	128
6.5	Hydrogen bound states studied by DFT	133
6.5.1	Computational details	133
6.5.2	Results	134
6.6	Discussion	142
6.7	Conclusion	145
7	Conclusions	147
7.1	Summary	147
7.2	Future work	149
7.2.1	Thermodynamic trends	149
7.2.2	Two-dimensional diffusion	150

7.2.3	Translational-rotational coupling	150
A	Effect of porous texture on hydrogen adsorption in activated carbons	151
A.1	Introduction	151
A.2	Experimental Methods	153
A.3	Results	155
A.4	Discussion	161
A.5	Conclusion	163
B	Hydrogen absorption behavior of the ScH₂-LiBH₄ system	164
B.1	Introduction	164
B.2	Experimental Details	166
B.3	Results	168
B.4	Discussion	174
B.5	Conclusion	175
	Bibliography	177

List of Figures

1.1	Phase diagram of molecular hydrogen	2
1.2	Optimizing the adsorption enthalpy with the Langmuir model	6
1.3	Illustration of dispersion interactions between two semi-infinite slabs	8
1.4	Structure of a hydrogen monolayer on graphene	14
1.5	Structures of MOF-5, zeolite A, and activated carbon	17
1.6	Maximum hydrogen adsorption capacities of various porous adsorbents plotted against their BET surface area	19
2.1	Isobars of the potassium-graphite system	23
2.2	Structure of the KC_{24} compound	24
2.3	Possible in-plane structures of the KC_{24} compound	27
2.4	Domain model for the CsC_{24} compound	28
2.5	Synthesized samples of KC_{24}	31
2.6	Powder XRD pattern of synthesized KC_{24} sample	32
2.7	Comparison of the powder XRD patterns from stage-1, stage-2, and stage-3 potassium graphite intercalation compounds	33
2.8	Comparison of of KC_{24} , RbC_{24} , and CsC_{24}	33
2.9	Raman spectra of potassium graphite intercalation compounds	35
2.10	Neutron diffraction patterns for a deuterated KC_{24} powder	37

2.11	Pair distribution function of deuterated KC_{24} at 35 K	38
3.1	Illustration of surface excess adsorption	41
3.2	Isosteric heat from fitting empirical functions separately to each isotherm . .	45
3.3	Isosteric heat from fitting to a single virial-type thermal equation	46
3.4	Differential enthalpy of adsorption in the Henry's law regime	48
3.5	Schematic illustration of the Sieverts instrument.	50
3.6	Correcting for empty reactor adsorption	54
3.7	Wavevectors and position vectors for a neutron scattering event	56
3.8	Typical geometry of a neutron scattering experiment	57
3.9	Schematic illustration of an inverse geometry neutron spectrometer and a di- rect geometry spectrometer	60
4.1	Hydrogen adsorption isotherms of a flake-graphite KC_{24} sample	63
4.2	Virial-type thermal equation fitted to the KC_{24} isotherm	64
4.3	Adsorption isotherms of a Grafoil-based KC_{24} sample	65
4.4	Hydrogen adsorption isotherms of an RbC_{24} sample	67
4.5	Hydrogen adsorption isotherms of an CsC_{24} sample	68
4.6	Hydrogen adsorption enthalpies for KC_{24} , RbC_{24} and CsC_{24}	68
4.7	Kinetics of hydrogen adsorption by RbC_{24}	69
5.1	Scattering law for continuous 2D diffusion	76
5.2	QENS spectra of $\text{KC}_{24}(\text{H}_2)_{0.5}$ between 80 K and 110 K	80
5.3	Hydrogen sublattice on KC_{24}	81
5.4	Linewidth of the honeycomb net model function plotted versus momentum transfer	84

5.5	QENS spectra at 80 K fitted to the honeycomb net jump diffusion model . . .	86
5.6	QENS spectra at 90 K fitted to the honeycomb net jump diffusion model . . .	87
5.7	QENS spectra at 100 K fitted to the honeycomb net jump diffusion model . . .	88
5.8	QENS spectra at 110 K fitted to the honeycomb net jump diffusion model . . .	89
5.9	Experimental $\text{KC}_{24}(\text{H}_2)_{0.5}$ spectra at 110 K fitted to the two-dimensional continuous diffusion model	91
5.10	The five largest momentum-transfer groups of the 110 K data	93
5.11	The QENS spectra of $\text{KC}_{24}(\text{H}_2)_{0.5}$ fitted to the FT-KWW function	95
5.12	Fit parameters for the FT-KWW function	96
5.13	Comparison of QENS spectra measured on DCS and HFBS spectrometers . . .	99
5.14	Elastic intensity scan of $\text{KC}_{24}(\text{H}_2)_1$ and $\text{KC}_{24}(\text{H}_2)_2$	100
5.15	Molecular dynamics trajectories of $\text{KC}_{28}(\text{H}_2)_1$	102
5.16	Mean square displacement from MD simulations at 70 K	104
5.17	Comparison of experimental and simulated hydrogen diffusion coefficients in $\text{KC}_{24}(\text{H}_2)_1$	106
5.18	Intermediate scattering functions calculated from MD trajectories	107
5.19	Effect of H_2 composition on QENS spectra of CsC_{24} at 65 K	108
5.20	Hydrogen diffusivity in various adsorbents compared to KC_{24}	109
6.1	Rotational energy level transitions for 1D hindered rotor model	117
6.2	Molecular form factors for pure rotational transitions of the H_2 molecule . . .	118
6.3	Low-energy-transfer IINS spectra of $\text{KC}_{24}(\text{H}_2)_x$	122
6.4	Decomposition of the low-energy-transfer IINS spectra of $\text{KC}_{24}(\text{H}_2)_x$ into a sum of Gaussian curves	123
6.5	Diffraction pattern of $\text{KC}_{24}(\text{H}_2)_x$ measured on DCS at 4 K.	125

6.6	Intermediate-energy IINS spectra of $\text{KC}_{24}(\text{pH}_2)_x$	127
6.7	High-energy IINS spectra of $\text{KC}_{24}(\text{pH}_2)_x$	129
6.8	Intermediate-energy IINS spectra of D_2 , HD, and $p\text{-H}_2$ adsorbed in KC_{24}	131
6.9	Comparison of the IINS spectra from $p\text{-H}_2$, HD, and D_2	132
6.10	Calculated potential energy surface for the KC_{28} unit cell	135
6.11	One-dimensional slices through the potential energy surface	137
6.12	Line scans for different H_2 orientations	138
6.13	Orientalional potential of H_2 in the theoretical KC_{28} structure	139
6.14	Transition energies for the anisotropic hindered rotor model	141
A.1	Surface texture analysis for the ACF-10 sample	154
A.2	High-resolution TEM image of the ACF-10 sample	156
A.3	Pore size distributions of the ACF-10, ACF-20, and CNS-201 samples, as determined by the DFT method	158
A.4	Hydrogen adsorption isotherms of ACF-10, ACF-20, and CNS-201	159
A.5	Isosteric heats measured for ACF-10, ACF-20, and CNS-201	161
B.1	Synthesis of scandium hydride	167
B.2	Kinetic desorption data for the $\text{ScH}_2 + 2\text{LiBH}_4$ system	169
B.3	Powder X-ray diffraction patterns for the $\text{ScH}_2 + 2\text{LiBH}_4$ system	171
B.4	NMR spectra of milled and dehydrogenated $\text{ScH}_2 + 2\text{LiBH}_4$	172
B.5	Comparison of the Raman spectra of dehydrogenated $\text{ScH}_2 + 2\text{LiBH}_4$ and neat LiBH_4	173

List of Tables

1.1	Current DOE revised technical targets for on-board hydrogen storage systems for light-duty vehicles	3
1.2	Major hydrogen storage methods	4
2.1	Lattice parameters of K, Rb, and Cs graphite intercalation compounds	34
3.1	Important definitions for adsorption	41
4.1	Hydrogen adsorption by KC_{24} , RbC_{24} , and CsC_{24}	66
5.1	Fit parameters for the honeycomb net jump diffusion model	90
5.2	Self-diffusion coefficients of $\text{KC}_{24}(\text{H}_2)_{0.5}$ determined from QENS	92
5.3	Jump diffusion residence times of $\text{KC}_{24}(\text{H}_2)_1$ measured on the DCS and HFBS spectrometers	99
6.1	Summary of peak positions and peak areas of the low-energy IINS spectra	124
6.2	Summary of peak positions and peak areas of the intermediate and high-energy IINS spectra	129
6.3	Comparison of peak positions of the intermediate IINS spectra for $p\text{-H}_2$, HD, and D_2 adsorbed in KC_{24}	132
6.4	Transition energies predicted by the one-dimensional hindered rotor model for various barrier heights	143

A.1	Surface texture parameters for ACF-10, ACF-20, and CNS-201	157
A.2	Hydrogen adsorption parameters for ACF-10, ACF-20, and CNS-201	160